

Article

Investigation on Deformation Mechanisms of NiTi Shape Memory Alloy Tube under Radial Loading

Shuyong Jiang ^{1,*}, Junbo Yu ², Li Hu ² and Yanqiu Zhang ¹

¹ College of Mechanical and Electrical Engineering, Harbin Engineering University, Harbin 150001, China; zhangyq@hrbeu.edu.cn

² College of Materials Science and Chemical Engineering, Harbin Engineering University, Harbin 150001, China; yujunbo@hrbeu.edu.cn (J.Y.); heu_huli@126.com (L.H.)

* Correspondence: jiangshuyong@hrbeu.edu.cn; Tel.: +86-451-8251-9710

Received: 9 June 2017; Accepted: 11 July 2017; Published: 13 July 2017

Abstract: NiTi shape memory alloy (SMA) tube was coupled with mild steel cylinder in order to investigate deformation mechanisms of NiTi SMA tubes undergoing radial loading. NiTi SMA tubes of interest deal with two kinds of nominal compositions; namely, Ni-50 at % Ti and Ni-49.1 at % Ti, where at room temperature, B19' martensite is dominant in the former, and B2 austenite is complete in the latter. The mechanics of the NiTi SMA tube during radial loading were analyzed based on elastic mechanics and plastic yield theory, where effective stress and effective strain are determined as two important variables that investigate deformation mechanisms of the NiTi SMA tube during radial loading. As for the NiTi SMA tube with austenite structure, stress-induced martensite (SIM) transformation as well as plastic deformation of SIM occur with the continuous increase of effective stress. As for NiTi SMA tube which possesses martensite structure, reorientation and detwinning of twinned martensite as well as plastic deformation of reoriented and detwinned martensite occur with the continuous increase in the effective stress. Plastic deformation for dislocation slip has a negative impact on superelasticity and shape memory effect of NiTi SMA tube.

Keywords: shape memory alloy; NiTi alloy; NiTi tube; radial loading; deformation mechanism

1. Introduction

NiTi shape memory alloy (SMA) has been substantially employed in the domain of engineering since it possesses perfect shape memory effect (SME) and excellent superelasticity [1]. Based on SME, NiTi SMA can remember the shape in the austenite phase when it is heated to austenite finish temperature (A_f) after undergoing a certain extent of deformation in the martensite state. In terms of superelasticity, NiTi SMA is characterized by nonlinear recoverable deformation behavior when the temperature is above A_f . Superelasticity stems from stress-induced martensite (SIM) transformation by exerting force and spontaneous reverse martensite transformation after removing force.

NiTi SMA tube—which possesses perfect SME, good corrosion resistance, high plateau stress, ultimate tensile strength, high fatigue life, and excellent superelasticity at/around body temperature—has been the best candidate for biomedical stents and pipe coupling [2–4]. More and more researchers have been engaged in plastic working of NiTi SMA tube, such as drawing [5–7], extrusion [8], spinning [9] and equal channel angular extrusion [10].

In particular, the mechanical behavior of NiTi SMA tube based on different loading modes is a critical factor in engineering applications. In general, NiTi SMA tube exhibits different mechanical behaviors as well as different transformation characteristics under different loading conditions. Sun and Li studied the mechanical behavior of B2 austenite NiTi SMA tube under simple tension and simple shear [11,12]. They found that when NiTi SMA tube with B2 austenite undergoes simple tension, SIM transformation occurs so that a martensitic spiral band can be observed. However, when NiTi

SMA tube with B2 austenite suffers from simple shear, a martensitic spiral band cannot be observed. SIM transformation of B2 austenite NiTi SMA tube under simple tension was further validated on the basis of experimental observation by Mao et al. [13]. Furthermore, Mao et al. also found that in the case of uniaxial compression, a homogeneous martensite phase transformation appears in B2 austenite NiTi SMA tube, where a martensitic spiral band is unable to be observed. Jiang et al. investigated buckling and recovery of B2 austenite NiTi SMA tube under compressive loading by combining digital image correlation (DIC) with finite element simulation, where SIM transformation plays a significant role [14,15]. Bechle and Kyriakides studied the mechanical behavior of B2 austenite NiTi SMA tube subjected to bending load. Consequently, they found that bending can also lead to localized nucleation of martensite phase, where deformation patterns exhibit the considerable difference between the compression and tension sides [16]. Wang et al. investigated the mechanical behavior of austenitic NiTi SMA tube subjected to biaxial load, which involves tension loading and torsion loading, and has been widely studied in the literature [17]. Bechle and Kyriakides also investigated localization evolution of B2 austenite NiTi SMA tube undergoing biaxial stress loading by means of DIC, which is able to track the evolution and degree of inhomogeneous deformation resulting from transformation from austenite into martensite under loading as well as from martensite into austenite under unloading [18,19]. Rivin et al. investigated the recoverable deformation of hollow thin-walled NiTi tube subjected to radial loading which acts on the outer wall of NiTi tube [20]. Zhang et al. studied the mechanical behavior of hollow thin-walled NiTi tube under radial quasi-static compression, where the compressive loading is also imposed on the outer wall of NiTi tube [21].

In the present study, a new radial loading mode is put forward for NiTi SMA tube by selecting mild steel cylinder as loading media. The radial loading is implemented by imposing inner pressure on the inner wall of NiTi tube, where inner pressure results from plastic deformation of the steel cylinder.

2. Materials and Methods

NiTi SMA bars—which have chemical composition of Ni-50 at % Ti and Ni-49.1 at % Ti, respectively—were used for manufacturing NiTi SMA tubes. The inner diameter, outer diameter, and height of NiTi SMA tubes were 8, 10, and 10 mm, respectively. In order to investigate the mechanical behavior and deformation mechanism, the mild steel cylinder (with diameter and height of 8 and 20 mm, respectively) was symmetrically inserted into NiTi SMA tube. The assembled sample experienced a compression test on the INSTRON-5500R equipment (Instron Corporation, Norwood, MA, USA), as shown in Figure 1. The pressure, p which is imposed on NiTi SMA tube can be solved according to plastic yield and plastic mechanics of the mild steel cylinder. The deformation mechanism of NiTi SMA tube can be analyzed based on the pressure p and according to the dimension variation during plastic deformation.



Figure 1. Photograph of NiTi shape memory alloy (SMA) tube undergoing radial loading test.

Microstructures of NiTi SMA samples were characterized using transmission electron microscope (TEM). Specimens for TEM experiment were mechanically ground to 70 μm . Subsequently, they were thinned via twin-jet polishing in an electrolyte composed of 6% HClO_4 , 34% $\text{C}_4\text{H}_{10}\text{O}$, and 60% CH_3OH , according to volume percentage. TEM observation was performed on a FEI TECNAI G2 F30 microscope (FEI Corporation, Hillsboro, OR, USA). To further acquire the microstructure of NiTi SMA samples, electron back-scattered diffraction (EBSD) experiments were carried out on NiTi SMA specimens using a Zeiss Supra 55 scanning electron microscope (University of South Carolina, Columbia, SC, USA) coupled with an OXFORD EBSD instrument (Oxford Instruments, Oxford, UK). The samples for EBSD were mechanically polished and subsequently electropolished in a solution of 30% HNO_3 and 70% CH_3OH by volume fraction at -30°C . A step size of 1.5 μm was used to capture area scans for NiTi SMA specimens.

3. Mechanical Analysis of NiTi SMA Tube under Radial Loading

The mechanical model of NiTi SMA tube under radial loading can be shown in Figure 2. NiTi SMA tube is viewed as the thick-walled tube under the action of the pressure p . The deformation mechanics of NiTi SMA tube belongs to the axisymmetric problem as well as the plane stress problem, where the axial stress σ_z is equal to zero without the axial loading, and the radial stress σ_r and the tangential stress σ_θ are irrespective of the axial coordinate axis. Simultaneously, it is assumed that all the total material particles within NiTi SMA tube experience deformation. σ_r and σ_θ are both the principal stresses due to the absence of shear stresses in NiTi SMA tube.

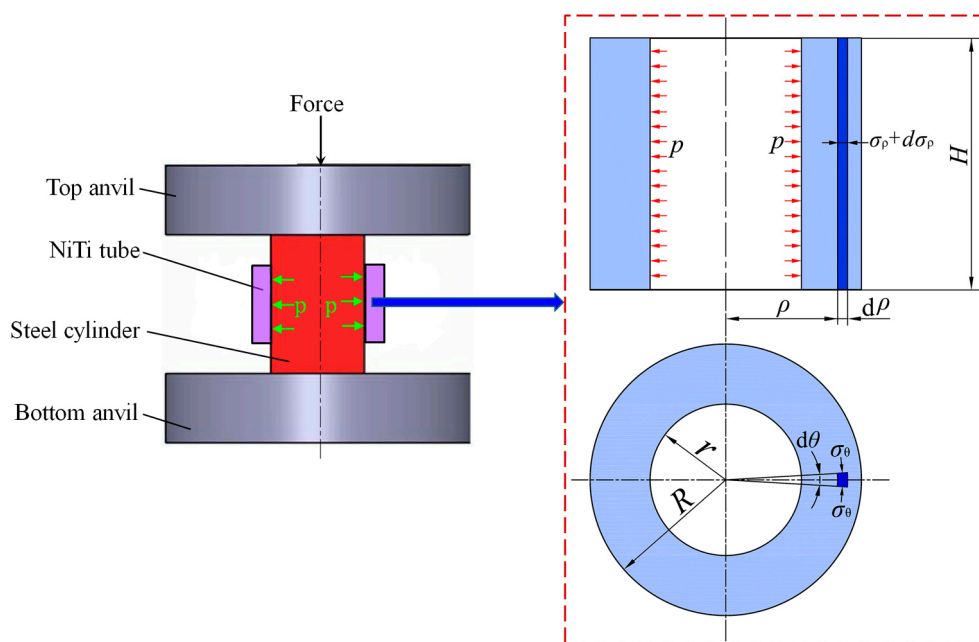


Figure 2. Mechanical model of NiTi SMA tube subjected to radial loading, where p is the pressure, R the outer radius, r the inner radius, and H the height.

3.1. Geometric Equation between Strain and Displacement

The tangential strain ε_θ and the radial strain ε_r of any point in NiTi SMA tube are expressed as follows, respectively

$$\begin{cases} \varepsilon_\rho = \frac{du}{d\rho} \\ \varepsilon_\theta = \frac{u}{\rho} \end{cases} \quad (1)$$

where u is the displacement of any point along the radius direction in NiTi SMA tube.

3.2. Equilibrium Equation under Static Inner Pressure

By intercepting an element slab in NiTi SMA tube in Figure 2, the equilibrium differential equation along the radial direction is obtained as follows.

$$(\sigma_\rho + d\sigma_\rho)(\rho + d\rho)hd\theta - \sigma_\rho h d\theta - 2\sigma_\theta \left(\sin \frac{d\theta}{2}\right)hd\rho = 0 \quad (2)$$

By ignoring the high-order items of Equation (2), the following equation can be obtained.

$$\frac{d\sigma_\rho}{d\rho} + \frac{\sigma_\rho - \sigma_\theta}{\rho} = 0 \quad (3)$$

3.3. Constitutive Equation between Stress and Strain

According to generalized Hooke's law, the relationship between the stresses and the strains can be expressed by

$$\begin{cases} \varepsilon_\rho = \frac{1}{E}(\sigma_\rho - \mu\sigma_\theta) \\ \varepsilon_\theta = \frac{1}{E}(\sigma_\theta - \mu\sigma_\rho) \end{cases} \quad (4)$$

Substitution of Equation (1) into Equation (4) results in

$$\begin{cases} \frac{du}{d\rho} = \frac{1}{E}(\sigma_\rho - \mu\sigma_\theta) \\ \frac{u}{\rho} = \frac{1}{E}(\sigma_\theta - \mu\sigma_\rho) \end{cases} \quad (5)$$

According to Equation (5), the expressions of σ_ρ and σ_θ can be expressed by

$$\begin{cases} \sigma_\rho = \frac{E}{1-\mu^2} \left(\frac{du}{d\rho} + \mu \frac{u}{\rho} \right) \\ \sigma_\theta = \frac{E}{1-\mu^2} \left(\frac{u}{\rho} + \mu \frac{du}{d\rho} \right) \end{cases} \quad (6)$$

Substitution of Equation (6) into Equation (3) leads to

$$\frac{d^2u}{d\rho^2} + \frac{1}{\rho} \frac{du}{d\rho} - \frac{u}{\rho^2} = 1 \quad (7)$$

The displacement u is obtained as follows by solving Equation (7).

$$u = \frac{1-\mu}{E} \frac{r^2 p \rho}{R^2 - r^2} + \frac{1+\mu}{E} \frac{r^2 R^2 p}{R^2 - r^2} \frac{1}{\rho} \quad (8)$$

Consequently, σ_ρ and σ_θ can be further expressed by

$$\begin{cases} \sigma_\rho = \frac{r^2 p}{R^2 - r^2} - \frac{r^2 R^2 p}{R^2 - r^2} \frac{1}{\rho^2} \\ \sigma_\theta = \frac{r^2 p}{R^2 - r^2} + \frac{r^2 R^2 p}{R^2 - r^2} \frac{1}{\rho^2} \end{cases} \quad (9)$$

The expressions for the radial strain, the tangential strain, and the axial strain ε_z are determined as follows.

$$\begin{cases} \varepsilon_\rho = \frac{1 - \mu}{E} \frac{r^2 p}{R^2 - r^2} - \frac{1 + \mu}{E} \frac{r^2 R^2 p}{R^2 - r^2} \frac{1}{\rho^2} \\ \varepsilon_\theta = \frac{1 - \mu}{E} \frac{r^2 p}{R^2 - r^2} + \frac{1 + \mu}{E} \frac{r^2 R^2 p}{R^2 - r^2} \frac{1}{\rho^2} \\ \varepsilon_z = -\frac{\mu}{E} \frac{2r^2 p}{R^2 - r^2} \end{cases} \quad (10)$$

The effective strain $\bar{\varepsilon}$ is expressed as follows.

$$\bar{\varepsilon} = \frac{\sqrt{2}}{3} \sqrt{(\varepsilon_\rho - \varepsilon_\theta)^2 + (\varepsilon_\theta - \varepsilon_z)^2 + (\varepsilon_z - \varepsilon_\rho)^2} \quad (11)$$

The axial stress σ_z is equal to zero due to the absence of loading along the axial direction. The effective stress is expressed as follows:

$$\bar{\sigma} = \frac{\sqrt{2}}{2} \sqrt{(\sigma_\rho - \sigma_\theta)^2 + (\sigma_\theta - 0)^2 + (0 - \sigma_\rho)^2} = \frac{\sqrt{2}}{2} \sqrt{(\sigma_\rho - \sigma_\theta)^2 + \sigma_\theta^2 + \sigma_\rho^2} \quad (12)$$

4. Results and Discussion

Figure 3 shows the microstructure of Ni-49.1 at % Ti SMA, which belongs to B2 austenite. The microstructure of Ni-50 at % Ti SMA is illustrated in Figure 4. It is found from Figure 4 that NiTi SMA belongs to B19' martensite, where martensite twins can be captured. Furthermore, the martensite twins belong to type I twins. It is generally accepted that type I twin plays a crucial role in SME of NiTi SMA.

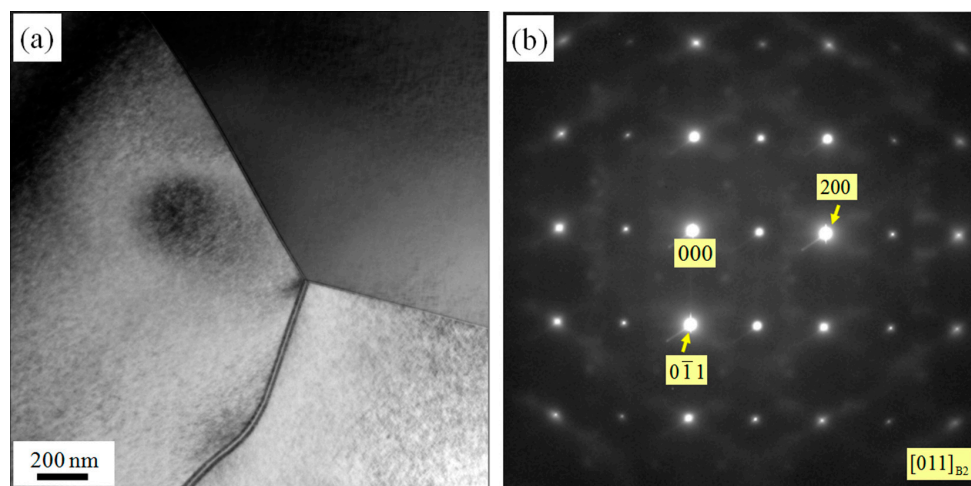


Figure 3. Transmission electron microscope (TEM) micrographs of Ni-49.1 at % Ti SMA: (a) bright field image; (b) diffraction pattern of (a).

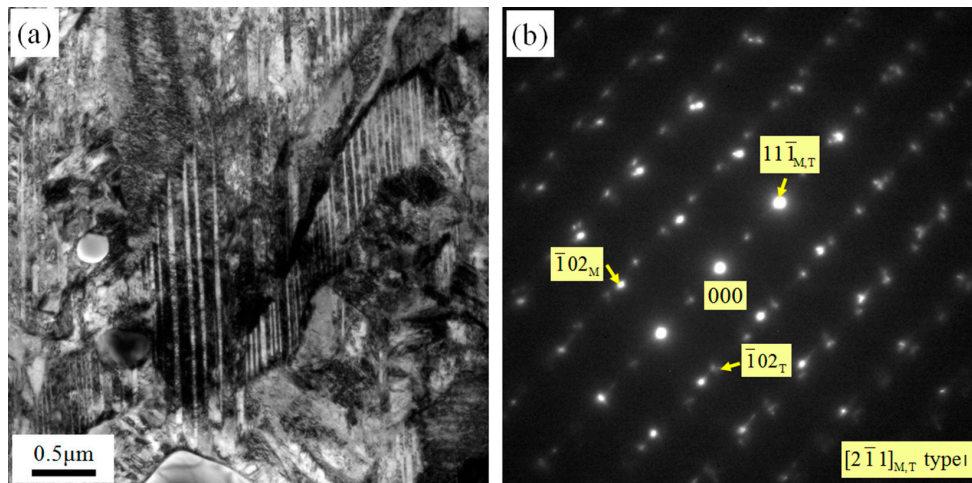


Figure 4. TEM micrographs of Ni-50 at % Ti SMA: (a) bright field image; (b) diffraction pattern of (a).

For the purpose of better understanding microstructure and phase composition of NiTi SMA, EBSD maps of Ni-49.1 at % Ti and Ni-50 at % Ti SMAs are shown in Figures 5 and 6, respectively. It can be found from Figure 5 that Ni-49.1 at % Ti SMA consists of complete B2 austenite structure. However, regarding Ni-50 at % Ti SMA, a small amount of residual B2 austenite appears in the matrix of B19' martensite. It is generally accepted that the residual B2 austenite phase has little influence on the mechanical behavior of Ni-50 at % Ti SMA. In other words, the mechanical behavior of Ni-50 at % Ti SMA is dominated by B19' martensite rather than B2 austenite. In addition, the distribution of twin boundaries can be observed in Figure 6a, and the frequency distributions of misorientation angles between B19' martensite and B19' martensite, as well as between B19' martensite and B2 austenite, are given in Figure 6b.

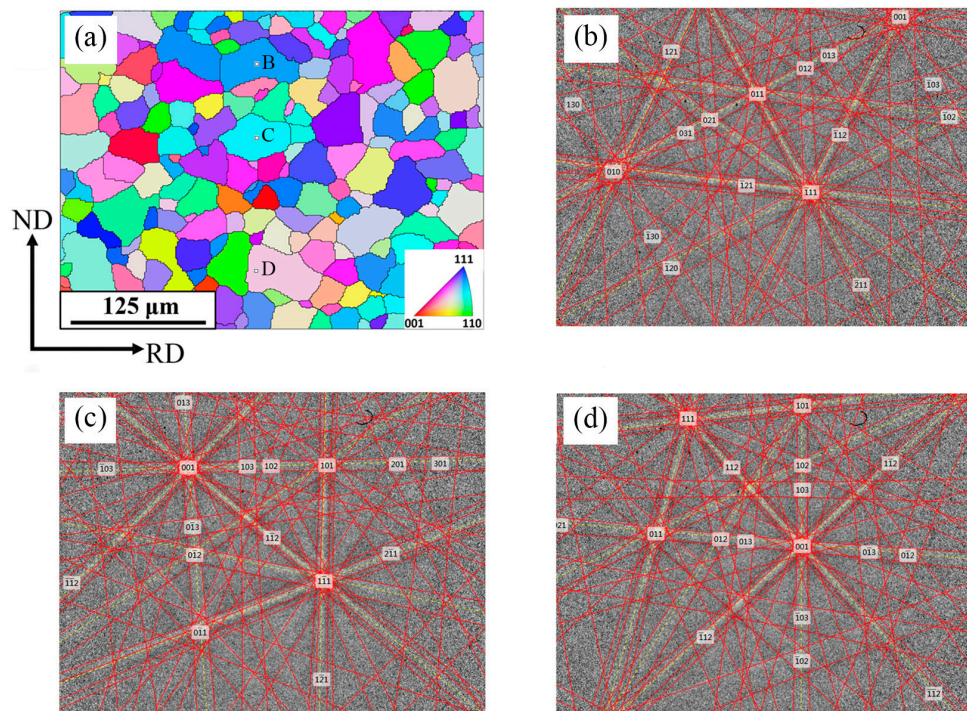


Figure 5. Electron back-scattered diffraction (EBSD) maps of Ni-49.1 at % Ti SMA: (a) microstructure; (b) kikuchi pattern of point B in (a); (c) kikuchi pattern of point C in (a); (d) kikuchi pattern of point D in (a).

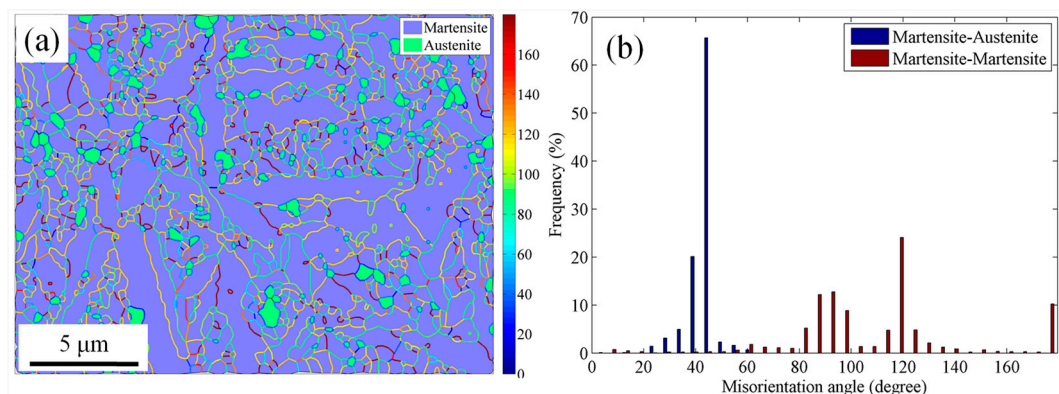


Figure 6. EBSD maps of Ni-50 at % Ti SMA: (a) microstructure; (b) frequency distribution of misorientation angle.

Figure 7 illustrates compression stress–strain curves of Ni-49.1 at % Ti and Ni-50 at % Ti SMAs, respectively. In general, in terms of compression loading, NiTi SMA with B2 austenite structure experiences elastic deformation of austenite, SIM transformation, elastic deformation of SIM, and plastic deformation of SIM based on dislocation slip [22]. However, in the case of compression loading, NiTi SMA with B19' martensite structure undergoes elastic deformation of twinned martensite, reorientation and detwinning of twinned martensite, elastic deformation of reoriented and detwinned martensite, and plastic deformation of reoriented and detwinned martensite based on dislocation slip [23,24].

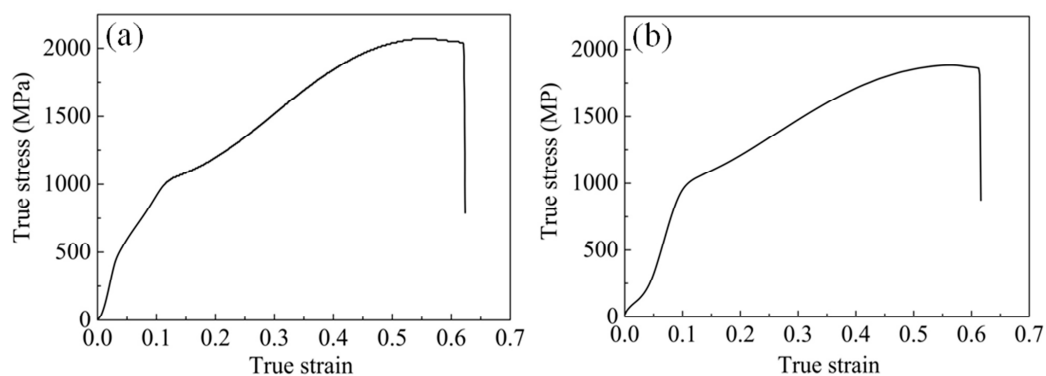


Figure 7. Compression stress–strain curves of NiTi SMAs: (a) Ni-49.1 at % Ti; (b) Ni-50 at % Ti.

According to the aforementioned mechanical analysis for NiTi SMA tube under radial loading, it can be accepted that the effective stress $\bar{\sigma}$ and the effective strain $\bar{\epsilon}$ become the two key parameters that analyze the mechanical behavior of NiTi SMA tube during radial loading. As for NiTi SMA tube with B2 austenite structure, when the effective stress $\bar{\sigma}$ is more than a critical value σ_{sim} above which SIM transformation can be induced, the crystal structure of NiTi SMA is converted from B2 structure to B19' structure, as shown in Figure 8. SIM transformation is of great significance in the superelastic behavior of NiTi SMA. Plastic deformation for dislocation slip—which has an adverse influence on superelasticity of NiTi SMA—occurs with the further progression of radial loading. As for NiTi SMA tube with B19' martensite structure, when the effective stress $\bar{\sigma}$ is greater than a critical value σ_{rd} above which reorientation and detwinning of twinned martensite is capable of arising, the crystal structure of NiTi SMA remains as B19' martensite, but the orientation of crystal exhibits a significant change, as shown in Figure 9. Reorientation and detwinning of twinned martensite lays a profound foundation for SME of NiTi SMA. With the further progression of radial loading, the plastic deformation of

reoriented and detwinned martensite for dislocation slip occurs, which has a negative impact on the SME of NiTi SMA. Consequently, dislocation slip should be avoided for NiTi SMA tube undergoing radial loading in order to guarantee the perfect SME of NiTi SMA tube.

So far, because of the limitation of experimental techniques, SIM transformation of NiTi SMA tube under radial loading has been unable to be validated by means of experimental observation. Martensitic reorientation and detwinning of NiTi SMA tube subjected to radial loading should be observed experimentally in the future.

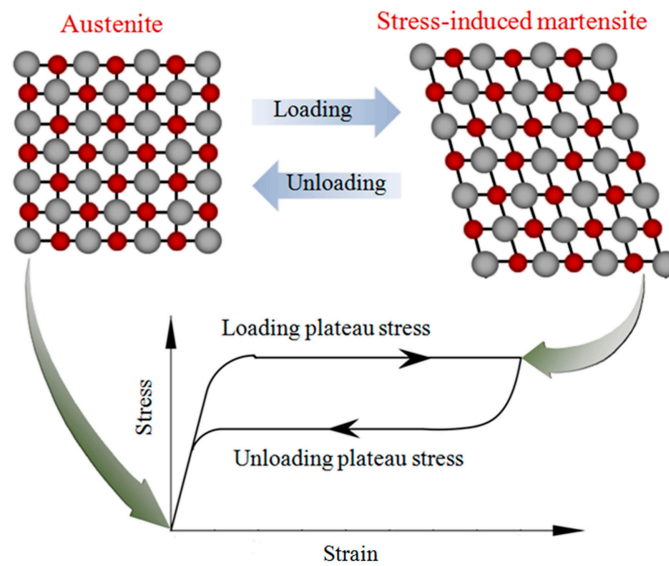


Figure 8. Schematic diagram of crystal structure evolution of NiTi SMA tube subjected to stress-induced martensite (SIM) transformation.

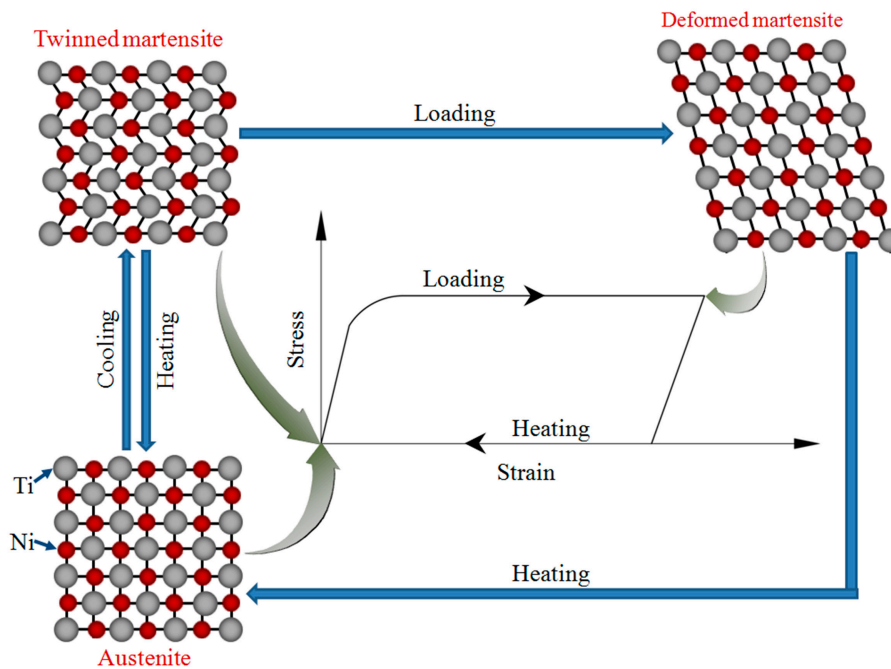


Figure 9. Schematic diagram of crystal structure evolution of NiTi SMA tube subjected to martensite reorientation and detwinning.

5. Conclusions

(1) A new radial loading mode is put forward for NiTi SMA tube, where NiTi SMA tube is subjected to the inner pressure which results from plastic deformation of the steel cylinder. The effective stress $\bar{\sigma}$ and the effective strain $\bar{\epsilon}$ are regarded as the two key parameters that analyze the mechanical behavior of NiTi SMA tube during radial loading. As for NiTi SMA tube with B2 austenite structure, when the effective stress $\bar{\sigma}$ is more than a critical value σ_{sim} above which SIM transformation can be induced, the crystal structure of NiTi SMA is converted from B2 structure to B19' structure. As for NiTi SMA tube with B19' martensite structure, when the effective stress $\bar{\sigma}$ is more than a critical value σ_{rd} above which reorientation and detwinning of twinned martensite is capable of arising, the crystal structure of NiTi SMA remains as B19' martensite, but the crystal orientation exhibits a significant change.

(2) When NiTi SMA tube is subjected to radial loading, SIM transformation is of great significance in the superelasticity of NiTi SMA, and reorientation and detwinning of twinned martensite lays a profound foundation for the SME of NiTi SMA. Plastic deformation for dislocation slip has an adverse influence on the superelasticity and SME of NiTi SMA tube. Because of the limitation of experimental techniques, SIM transformation of NiTi SMA tube under radial loading has been unable to be validated by means of TEM observation since shape recovery of NiTi SMA tube can occur after unloading. Martensitic reorientation and detwinning of NiTi SMA tube subjected to radial loading should be observed by means of TEM techniques, since shape recovery of NiTi SMA tube cannot occur after unloading. We will perform the corresponding investigation in the future.

Acknowledgments: The work was financially supported by National Natural Science Foundation of China (Nos. 51475101, 51305091 and 51305092).

Author Contributions: Shuyong Jiang wrote the manuscript; Junbo Yu performed EBSD analysis; Li Hu performed TEM analysis; Yanqiu Zhang performed mechanical analysis.

Conflicts of Interest: The authors declare no conflict of interest.

References

- Otsuka, K.; Ren, X. Physical metallurgy of Ti–Ni-based shape memory alloys. *Prog. Mater. Sci.* **2005**, *50*, 511–678. [[CrossRef](#)]
- Robertson, S.W.; Ritchie, R.O. In vitro fatigue–crack growth and fracture toughness behavior of thin-walled superelastic Nitinol tube for endovascular stents: A basis for defining the effect of crack-like defects. *Biomaterials* **2007**, *28*, 700–709. [[CrossRef](#)] [[PubMed](#)]
- Jee, K.; Han, J.; Jang, W. A method of pipe joining using shape memory alloys. *Mater. Sci. Eng. A* **2006**, *438*, 1110–1112. [[CrossRef](#)]
- Wang, L.; Rong, L.; Yan, D.; Jiang, Z.; Li, Y. DSC study of the reverse martensitic transformation behavior in a shape memory alloy pipe-joint. *Intermetallics* **2005**, *13*, 403–407. [[CrossRef](#)]
- Wu, M.H. Fabrication of nitinol materials and components. *Mater. Sci. Forum* **2002**, 285–292. [[CrossRef](#)]
- Yoshida, K.; Watanabe, M.; Ishikawa, H. Drawing of Ni–Ti shape-memory-alloy fine tubes used in medical tests. *J. Mater. Process. Technol.* **2001**, *118*, 251–255. [[CrossRef](#)]
- Yoshida, K.; Furuya, H. Mandrel drawing and plug drawing of shape-memory-alloy fine tubes used in catheters and stents. *J. Mater. Process. Technol.* **2004**, *153*, 145–150. [[CrossRef](#)]
- Müller, K. Extrusion of nickel–titanium alloys Nitinol to hollow shapes. *J. Mater. Process. Technol.* **2001**, *111*, 122–126. [[CrossRef](#)]
- Jiang, S.Y.; Zhang, Y.Q.; Zhao, Y.N.; Tang, M.; Li, C.F. Finite element simulation of ball spinning of NiTi shape memory alloy tube based on variable temperature field. *Trans. Nonferrous Met. Soc. China* **2013**, *23*, 781–787. [[CrossRef](#)]
- Jiang, S.Y.; Zhao, Y.N.; Zhang, Y.Q.; Tang, M.; Li, C.F. Equal channel angular extrusion of NiTi shape memory alloy tube. *Trans. Nonferrous Met. Soc. China* **2013**, *23*, 2021–2028. [[CrossRef](#)]
- Sun, Q.-P.; Li, Z.-Q. Phase transformation in superelastic NiTi polycrystalline micro-tubes under tension and torsion—from localization to homogeneous deformation. *Int. J. Solids Struct.* **2002**, *39*, 3797–3809. [[CrossRef](#)]

12. Li, Z.; Sun, Q. The initiation and growth of macroscopic martensite band in nano-grained niti microtube under tension. *Int. J. Plast.* **2002**, *18*, 1481–1498. [[CrossRef](#)]
13. Mao, S.; Luo, J.; Zhang, Z.; Wu, M.; Liu, Y.; Han, X. Ebsd studies of the stress-induced B2–B19' martensitic transformation in NiTi tubes under uniaxial tension and compression. *Acta Mater.* **2010**, *58*, 3357–3366. [[CrossRef](#)]
14. Jiang, D.; Bechle, N.J.; Landis, C.M.; Kyriakides, S. Buckling and recovery of NiTi tubes under axial compression. *Int. J. Solids Struct.* **2016**, *80*, 52–63. [[CrossRef](#)]
15. Jiang, D.; Landis, C.M.; Kyriakides, S. Effects of tension/compression asymmetry on the buckling and recovery of NiTi tubes under axial compression. *Int. J. Solids Struct.* **2016**, *100*, 41–53. [[CrossRef](#)]
16. Bechle, N.J.; Kyriakides, S. Localization in NiTi tubes under bending. *Int. J. Solids Struct.* **2014**, *51*, 967–980. [[CrossRef](#)]
17. Wang, Y.; Yue, Z.; Wang, J. Experimental and numerical study of the superelastic behavior on NiTi thin-walled tube under biaxial loading. *Comput. Mater. Sci.* **2007**, *40*, 246–254. [[CrossRef](#)]
18. Bechle, N.J.; Kyriakides, S. Evolution of localization in pseudoelastic NiTi tubes under biaxial stress states. *Int. J. Plast.* **2016**, *82*, 1–31. [[CrossRef](#)]
19. Bechle, N.J.; Kyriakides, S. Evolution of phase transformation fronts and associated thermal effects in a NiTi tube under a biaxial stress state. *Extreme Mech. Lett.* **2016**, *8*, 55–63. [[CrossRef](#)]
20. Rivin, E.I.; Sayal, G.; Singh Johal, P.R. “Giant superelasticity effect” in NiTi superelastic materials and its Applications. *J. Mater. Civ. Eng.* **2006**, *18*, 851–857. [[CrossRef](#)]
21. Zhang, K.; Zhang, H.J.; Tang, Z.P. Experimental study of thin-walled TiNi tubes under radial quasi-static compression. *J. Intell. Mater. Syst. Struct.* **2011**, *22*, 2113–2126.
22. Elibol, G.; Wagner, M.F.X. Investigation of the stress-induced martensitic transformation in pseudoelastic NiTi under uniaxial tension, compression and compression–shear. *Mater. Sci. Eng. A* **2015**, *621*, 76–81. [[CrossRef](#)]
23. Liu, Y.; Xie, Z.; Van Humbeeck, J.; Delaey, L. Asymmetry of stress-strain curves under tension and compression for NiTi shape memory alloys. *Acta Mater.* **1998**, *46*, 4325–4338. [[CrossRef](#)]
24. Liu, Y.; Xie, Z.; Van Humbeeck, J.; Delaey, L. Some results on the detwinning process in NiTi shape memory alloys. *Scr. Mater.* **1999**, *41*, 1273–1281. [[CrossRef](#)]



© 2017 by the authors. Licensee MDPI, Basel, Switzerland. This article is an open access article distributed under the terms and conditions of the Creative Commons Attribution (CC BY) license (<http://creativecommons.org/licenses/by/4.0/>).